Applied Physics Letters ARTICLE scitation.org/journal/apl

X-ray-induced acoustic computed tomography (XACT) imaging with single-shot nanosecond x-ray

Cite as: Appl. Phys. Lett. **119**, 183702 (2021); doi: 10.1063/5.0071911
Submitted: 17 September 2021 · Accepted: 12 October 2021 ·
Published Online: 2 November 2021

View Online Export Citation CrossMark

Siqi Wang,[1] Vassili Ivanov,[2] Prabodh Kumar Pandey,[3] and Liangzhong Xiang[1,3,4,a)]

AFFILIATIONS

[1]The Department of Biomedical Engineering, University of California, Irvine, California 92617, USA
[2]PhotoSound Technologies Inc., Houston, Texas 77036, USA
[3]The Department of Radiological Sciences, University of California, Irvine, California 92617, USA
[4]Beckman Laser Institute & Medical Clinic, University of California, Irvine, California 92612, USA

[a)]Author to whom correspondence should be addressed: liangzhx@hs.uci.edu

ABSTRACT

X-ray-induced acoustic computed tomography (XACT) has emerged as a promising imaging modality with broad applications in both biomedicine and nondestructive testing. The previous XACT imaging systems require thousands of averages to achieve reasonable images. Here, we report the experimental demonstration of single-shot XACT imaging of a metal object using a single-shot 50 ns x-ray pulse. A two-stage dedicated amplification and a 128-channel parallel data acquisition configuration were introduced for XACT imaging to enable sufficient acoustic signal amplification and maintain an overall low noise level for single-shot XACT imaging. Details of the system design are presented; the improved signal-to-noise ratio (>23 dB) and image reconstruction have been demonstrated with a ring ultrasound transducer array imaging system. The study paves the way for realizing real-time XACT imaging and its potential applications in image-guided intervention.

X-ray-induced acoustic computed tomography (XACT) as an imaging modality has shown great potential in applications ranging from biomedical imaging to nondestructive testing.[1–5] XACT is unique because it combines the x ray's advantage of high contrast and high-resolution character from ultrasound-based reception.[1] Over the past few years, XACT system implementations have been explored by different research groups. In the field of biomedicine, early proposals of XACT employments demonstrated the potential of XACT in mammography as a feasible lower-dose computed tomography (CT) alternative to x-ray CT.[2,3,6–8] Due to the fact that x-ray-induced acoustic (XA) signal is directly proportional to the absorbed radiation dose, XACT has also been brought up for its potential employment in radiation dosimetry and real-time radiation therapy monitoring.[8–10] In the field of nondestructive testing, XACT technology has also been actively discussed due to its relatively high-resolution potential, ease of operation, and versatile placement.[1,5]

In XACT, nanosecond to microsecond x-ray pulses are utilized to induce the x-ray acoustic (XA) effect, which describes the process of x-ray photons being absorbed by inner-shell electrons of the target medium, resulting in the release of photoelectrons.[4,6,11] The energy transfer process of the XA effect causes subsequent temperature increases. Upon satisfying the thermal and elastic confinement requirement, the temperature change can be localized. The initial pressure that is necessary for ultrasound wave propagation is then generated due to the atomic-level vibration following the localized temperature change.[4,12] The generated ultrasound wave can propagate omnidirectionally from the point of its generation. Thus, in theory, a three-dimensional (3D) reconstruction of the target medium can be obtained from a single pulse of x ray. However, in experimental settings, typical x-ray-induced acoustic initial pressures are considerably smaller in amplitude than that of typical ultrasound wave pressures.[5] Because of the lack of consideration for such low-pressure level acoustic waves in the signal conditioning path of currently available commercial signal acquisition systems, some of the generated ultrasound waves cannot be sufficiently amplified to meet the requirement of the minimum detectable voltage of the digital-to-analog converter (DAQ). Moreover, without effective conditioning, the input-inferred noise level is relatively high compared with the detected XA signals lowering

the overall signal-to-noise ratio (SNR) of the digitized signals. In previous studies, extensive signal averaging and prolonged scanning time were needed to overcome the limitation and obtain a satisfactory signal-to-noise ratio (SNR).[2,10,13,14] A 2D XACT reconstruction with a ring-array ultrasound transducer was introduced by Tang *et al.* in 2017 using more than 3800 x-ray pulse averages.[13] In 2020, a 3D XACT imaging of lead structures was achieved by rotating an arc-shape ultrasound array with 180 × 15 (rotation steps × average frames per step) total x-ray pulses.[14] In the same year, XACT combined with traditional ultrasound imaging, a dual modality system concept, was explored by Zhang *et al.* During the XA signal acquisition, 440 x-ray pulses were needed to reach 2:1 SNR on the A-scan XA signals.[15] To further the development of XACT technology, reconfiguring the signal path of the existing ultrasound acquisition system so that the low-pressure level acoustic waves from the XA effect can be sufficiently digitized is crucial to achieving XACT imaging with a single x-ray pulse.

In this paper, we demonstrated single-shot XACT imaging by using a 50 ns x-ray pulse with submillimeter resolution. A 2D XACT reconstruction was realized with a single x-ray pulse. A configuration of a 128-channel ultrasound signal acquisition system and its two-stage amplification configuration have been introduced. The configuration of the developed system largely improved the sensitivity of the XACT imaging when compared to the XACT imaging systems previously reported.

To demonstrate the performance of the proposed two-stage amplification and DAQ system in XACT, a "T" shaped 1/64-in.-thick lead sample fixed at the center of a water-based phantom 3% Agar (Bacto^{TM}, Becton, Dickinson and Company, NJ, USA) concentration was used as the imaging target. The schematic of the XACT experimental setup is shown in Fig. 1(a). A battery-powered pulsed x-ray generator (XR200, Golden Engineering, IN, USA) was placed right beneath the ring array, projecting x-ray beams upward to excite the imaging target. The x-ray generator operates at a tube energy of 150 KVp and is capable of sending out x-ray pulses at a repetition rate of 10 Hz with a 50 ns pulse width. The average output dose is rated a 2.6 mR/pulse at 12 in. with a projection angle of 40°. During the experiment, the x-ray pulsing is controlled by a remote outside of an x-ray radiation shielding cage. A Ce: Lu_2SiO_5 crystal (MTI Corporation, CA, USA) placed above the water tank was used as a scintillator to convert x-ray photons to visible light photons. An integrated amplified photodetector (APD410C, Thorlabs, NJ, USA) detects the visible light trigger pulse and sends the pulse to the three-stage amplification and DAQ system. To account for the time delays after x-ray pulses from

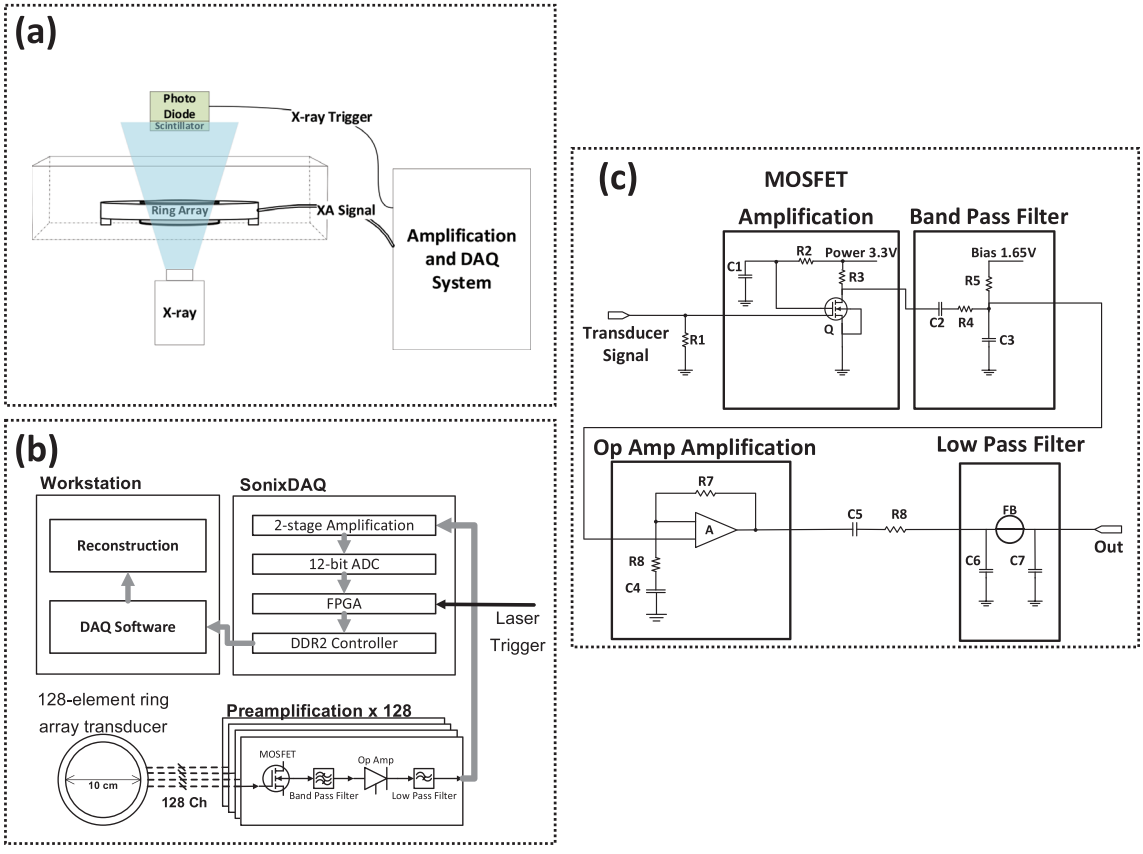

FIG. 1. (a) Diagram of the system setup for the XACT imaging experiment with single nanosecond x-ray pulse; (b) schematic diagram of the developed ultrasound acquisition scheme with added preamplification stage. (c) Circuit schematic of the four-stage 128-channel preamplification.

the scintillator, the photodiode, the preamplification stage and the SonixDAQ, a total of 4.625 μs of delay compensation was employed during reconstruction.

Figure 1(b) gives a flow chart illustration of the developed multi-channel data acquisition system connected to a custom-designed 128-channel ultrasonic ring array (PA probe, Doppler Co. Limited, Guangzhou, China) transducer. The system is consisting of three data transformation stages: the preamplification stage, the integrated amplification stage, and the analog-to-digital conversion stage. In the first pre-amplification stage, the raw 128-channel acoustic information will first go through a customized 128-channel preamplifier with a low input-referred noise figure. The preamplification stage was designed to convert the weak raw acoustic signals into output-ready signals that are strong enough to be noise-tolerant and detectable by the main stage of amplification. The preamplifier described in Fig. 1(b) has four internal sub-stages for each channel path [Fig. 1(c)]. The two amplification sub-stages are powered from a single 3.3 V rail. The transducer signal input is DC coupled to the common ground, which is set as zero by the input resistor R1. The other function of the input resistor is setting the input impedance of the MOSFET amplification stage. The MOSFET amplification substage uses a dual-gate and zero-bias MOSFET (BF908, NXP Semiconductors N.V., Eindhoven, Netherlands) in an open-loop configuration. Then, the MOSFET amplification stage is followed by an RC (resistance and capacitance) bandpass filter stage, with operational amplifier bias voltage supplied through the R5 resistor. The Op-amp stage is formed by an operational amplifier (ADA4895, Analog Devices, MA, USA) in an inverting configuration with the gain set by R7 and R6 resistors. The capacitor C5 is the decoupling capacitor, and the resistor R8 sets the output impedance. Due to the high-frequency impedance characteristics of the ferrite bead used (HZ0402A601R-10, Laird, MO, USA), the designed final low-pass filter (LPF) is steeper than a typical linear CLC (capacitor– inductor–capacitor) Pi-filter.

The conditioned acoustic signals then enter the data acquisition device (SonixDAQ, DK Medical, Canada) and travel through another two-stage amplification that is integrated into the DAQ system. The integrated amplification has a total of 52 dB gain. Combined with the 40 dB amplification from the multi-channel preamplifier, the final signal strength will be adequate for XACT experiments. After the second amplification stage, the 128-channel analog acoustic information is then sampled and converted to digital values by the onboard 12-bit analog-to-digital converters (ADCs). In continuous scanning mode, the digital data are temporarily stored in the internal DDR2 (Double Data Rate, Version 2) synchronous Dynamic Random-Access Memory (SDRAM) and then transferred to the host workstation computer via the universal serial bus (USB) interface.

Once the acquisition and digitization of the ultrasound signals are finished, the digital data are downloaded to the hard disk of the workstation computer by calling a loader program. The program provides a graphical user interface (GUI), the acquisition settings, and single-frame displays for the DAQ device.

During the XACT imaging with single-shot nanosecond x-ray experiment, the SonixDAQ system was set to acquire 2700 samples per trigger signal at a sampling rate of 40 MHz, which translates to approximately 10 cm XA wave travel distance and 67.5 μs sound travel time in the water to cover the entire ultrasound transducer ring array's region of interest (ROI). A total of 96 frames in which each frame consists of 128 channels of XA wave information were taken for the test, and frame number 8 was chosen to be processed for single x-ray pulse reconstruction for the XACT single x-ray pulse reconstruction demonstration. For post-processing, a digital lowpass filter with a 3 MHz cut-out frequency and a –90 dB attenuation strength was employed for the acquired XA signals. In addition, a universal back-projection algorithm-based MATLAB reconstruction program was used for the image reconstruction of this demonstration.[16]

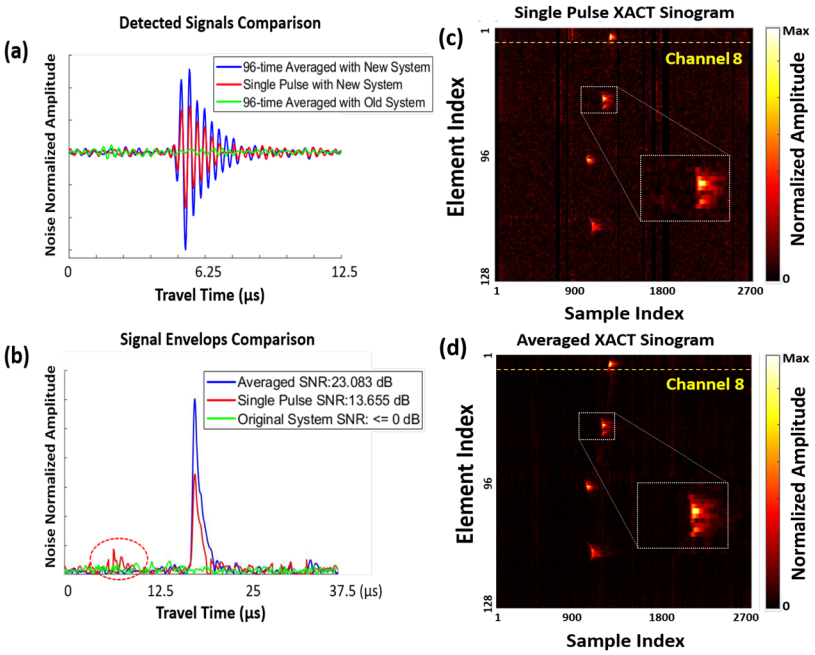

FIG. 2. (a) Overlay of detected signals using the proposed configuration with a preamplification stage vs the original configuration. (b) Overlay of corresponding signal envelops with calculated SNR values. The dashed red circle indicates the random noise ripple from electromagnetic interference (EMI). (c) The obtained sinogram from the proposed ultrasound acquisition configuration. (d) The obtained sinogram from the original ultrasound acquisition configuration.

Figure 2(a) demonstrates an overlay of detected XA signals using the original system configuration and the upgraded system within a 12.5 μs window cropped out of the 67.5 μs total signal travel time from 2700 samples. All three signals were collected from channel number 8 indicated in Fig. 2(c), with the same time window crop and the same target/ring array orientation. The signal amplitudes are noise normalized such that all three resulting signals have the same average noise floor amplitudes. Due to the higher averaged count with the 96-time averaged signal, the random noises in the averaged signal were further minimized, which resulted in higher signal SNR. With normalized noise floor in the signal comparison plot, the higher SNR makes the 96-average signal appeared to have bigger amplitude comparing with the single-pulse plot. The green signal plot in Fig. 2(a) indicates the 96-time averaged XA signals using the original system. Within the time window, no XA signal peak could be identified, due to the insufficient amplification design of the original configuration. The red XA signal plot indicates the XA signal extracted from the same channel using a single pulse of x-ray acquired by the developed two-stage amplification DAQ system. An XA signal spike starting from 6 μs can be clearly identified. Finally, the blue-colored signal plot showcases the averaged XA signal using 96 x-ray pulses acquired by the developed two-stage amplification DAQ system. A further SNR improvement can be noticed thanks to the additional noise reduction with 96-time averaging.

For a more direct signal comparison visualization and signal quality quantification, the envelopes of all three signals are extracted using Hilbert transformation [Fig. 2(b)]. A larger time window was chosen to include the noise ripple caused by EMI (indicated in dashed red circle) on the single pulse signal envelop plot. With a 96-time average, random noise interference can be reduced. Thus, the averaged signal plot yielded an enhanced SNR of 23.083 dB. Since identifiable XA signals were not found in the averaged signal acquired by the first-generation system, the SNR for the original system's signal is considered to be equal or smaller than the noise floor, which indicates an SNR of $<= 0$ dB.

In Fig. 2(c), the acquired single-pulse XACT sinogram and the averaged XACT sinogram were shown to demonstrate the signal quality across the channels and the noise-reduction effect with the averaged frames. One part of the XACT signals was magnified in each sinogram for close-up inspections. Although one frame sinogram already yields adequate SNR, the 96-pulse averaged sinogram demonstrated improved background-signal contrast and revealed even smaller signals previously buried in noises [Fig. 2(d)].[13]

In addition to sinograms, the back-projection-based reconstruction results are shown in Figs. 3(a) and 3(b) for single-frame and averaged reconstructions, respectively. A picture of the T shaped lead alongside a ruler for size reference was captured before being embedded into the agar-based phantom [Fig. 3(c)]. Two-line profiles perpendicular to the target line were taken to estimate the system resolving power by using the full-wave half maximum (FWHM) method with or without average. Figures 3(d) and 3(e) show the extracted line profiles and the overlaid Gaussian curve fitting the line profiles. The FWHM estimated for the single frame reconstruction along the dashed line was 1.24 mm. The averaged reconstruction showed minor improved, and the FWHM was estimated to be 0.975 mm.

The introduced XACT configuration sufficiently amplified digitized XA signals were revealed with a single x-ray pulse from a portable radiation source. One problem that the developed sensitivity

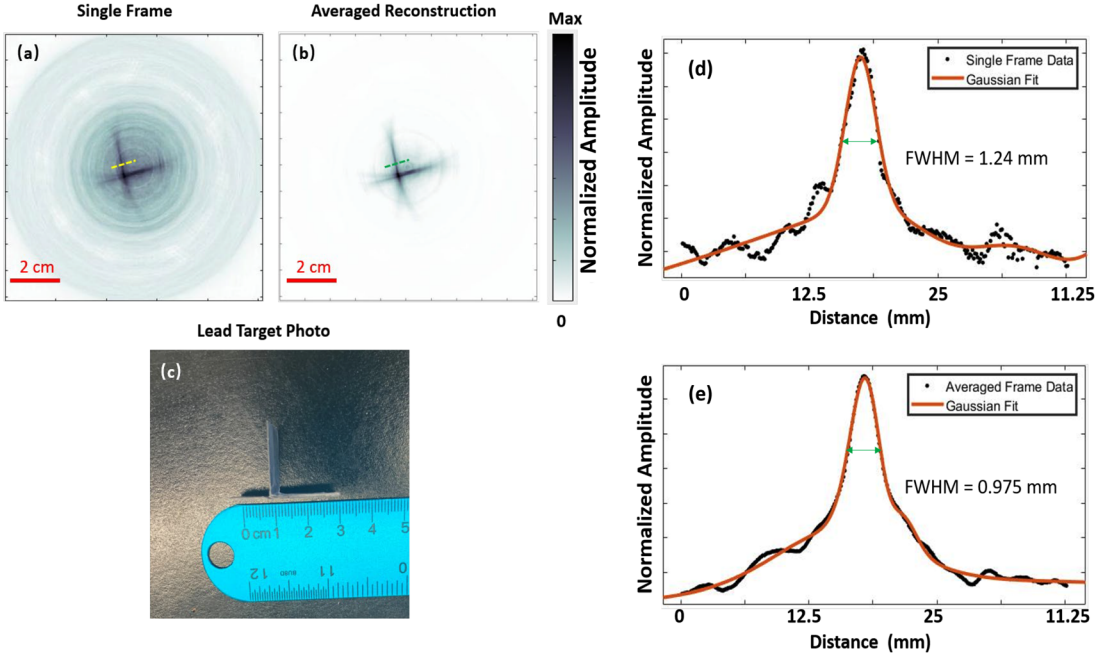

FIG. 3. (a) XACT reconstruction of the target from a single x-ray pulse. (b) XACT reconstruction of the target from averaged XA signals with 96 x-ray pulses. (c) Picture of the imaged T shaped lead target. (d) FWHM plot with fitted Gaussian curve based on the single x-ray pulse reconstruction data. (e) FWHM plot with fitted Gaussian curve based on the 96-frame reconstruction data.

enhanced fast XACT imaging system configuration aims to solve is enabling XACT imaging with reduced frame averaging. In 2017, Tang *et al.* reported that more than 4000 frames were required to generate a 2D reconstruction with sufficient image quality, using the same ultrasound transducer ring array. The signal comparison test demonstrated that the developed fast XACT imaging system has greatly enhanced sensitivity, and the requirement for x-ray pulse average is drastically reduced. The study paves the way for realizing real-time XACT imaging applications.

Although single x-ray pulse reconstructions can now be realized with the demonstrated system, averaged frame reconstruction still shows improvements in SNR and resolution. However, both estimated FWHMs are off from the ground truth 1/64 thickness of the lead target. It is likely that using a more accurate reconstruction method other than the basic universal back-projection reconstruction method used, like delay-and-sum, or model-based reconstruction algorithm, will improve the overall system resolution.[17–19]

Moreover, to further improve the sensitivity of the XACT system, the currently standalone preamplifier can be integrated into the ultrasound detectors for the next generation XACT imaging system.[20,21] With the front-end integrated transducer amplification design, the electromagnetic interference between channels and the signal quality degradation along transmission cables will be reduced. In addition, frontend electronics can provide local pulsing, amplification, filtering, and signal digitization, paving the way toward achieving a compact portable XACT 3D scanning all-in-one system.

This study has demonstrated that XACT imaging in 2D can be achieved using the acoustic characterization of a 128-channel ring array transducer with the sensitivity enhanced fast XACT imaging system, with a single 50-ns x-ray pulse. The proposed configuration can sufficiently prepare the raw XA signals for further post-processing. An XACT signal comparison test was conducted to demonstrate the improvement in system sensitivity over the original configuration. With improved amplification, the sensitivity enhanced fast XACT imaging system can achieve a high signal-to-noise ratio and reveal noise-buried weak XA signals. Moreover, the reconstruction quality of the developed system has been evaluated by performing an XACT ring-array scan. With higher XA signal strength, the total x-ray pulses needed for XACT signal averaging were drastically reduced, which in turn reduces the overall dosage to the imaging target and shortens the scanning time.

In summary, we developed and validated an ultrasound acquisition configuration that offers high-resolution XACT imaging from a single nanosecond x-ray pulse. Using the 128-channel ring-shaped ultrasound array and the 150 KvP x-ray source with 50 ns pulse width, full tomographic imaging capability from a single pulse with a spatial resolution of 0.97 mm can be achieved. The system configuration and the methodology introduced in this Letter can be utilized for dynamic monitoring of clinical treatments and planning, such as the needle movement during Brachytherapy. Moreover, the study validates that a sophisticated preamplification design is beneficial and necessary for the XACT system in addition to traditional ultrasound acquisition systems. This study paves the way for XACT imaging to be used for clinical studies for real-time monitoring of clinical activities.

Research reported in this publication was supported by the National Cancer Institute of the National Institutes of Health under Award Number (R37CA240806). The content is solely the responsibility of the authors and does not necessarily represent the official views of the National Institutes of Health. Approximately, $500k of federal funds supported the effort (50%) on this project. Approximately, $200k of American Cancer Society (133697-RSG-19-110-01-CCE) funds supported a portion of the effort (45%) on this project. The authors would like to acknowledge the support from UCI Chao Family Comprehensive Cancer Center (P30CA062203) (3%) and seed grant from school of medical at UCI(2%).

AUTHOR DECLARATIONS

Conflict of Interest

The authors have no conflicts of interest to disclose.

DATA AVAILABILITY

The data that support the findings of this study are available from the corresponding author upon reasonable request.

REFERENCES

[1]S. Tang, C. Ramseyer, P. Samant, and L. Xiang, Appl. Phys. Lett. **112**, 063504 (2018).
[2]S. Choi, D. Lee, E.-Y. Park, J.-J. Min, C. Lee, and C. Kim, Proc. SPIE **11240**, 112404R (2020).
[3]S. Tang, K. Yang, Y. Chen, and L. Xiang, Med. Phys. **45**, 1662 (2018).
[4]S. Wang *et al.*, Geofluids **2019**, 5485731.
[5]P. Samant, L. Trevisi, X. Ji, and L. Xiang, Photoacoustics **19**, 100177 (2020).
[6]L. Xiang, B. Han, C. Carpenter, G. Pratx, Y. Kuang, and L. Xing, Med. Phys. **40**, 010701 (2013).
[7]E. Robertson, P. Samant, S. Wang, T. Tran, X. Ji, and L. Xiang, IEEE Trans. Ultrason., Ferroelectr., Freq. Control **68**, 1073 (2021).
[8]S. Hickling, L. Xiang, K. C. Jones, K. Parodi, W. Assmann, S. Avery, M. Hobson, and I. E. Naqa, Med. Phys. **45**, e707 (2018).
[9]H. Lei, W. Zhang, I. Oraiqat, Z. Liu, J. Ni, X. Wang, and I. E. Naqa, Med. Phys. **45**, 4191 (2018).
[10]S. Hickling, H. Lei, M. Hobson, P. Léger, X. Wang, and I. E. Naqa, Med. Phys. **44**, 608 (2017).
[11]M. E. Garcia, G. M. Pastor, and K. H. Bennemann, Phys. Rev. Lett. **61**, 121 (1988).
[12]Y. Zhou, J. Yao, and L. V. Wang, J. Biomed. Opt. **21**, 061007 (2016).
[13]S. Tang, D. H. Nguyen, A. Zarafshani, C. Ramseyer, B. Zheng, H. Liu, and L. Xiang, Appl. Phys. Lett. **110**, 103504 (2017).
[14]D. Lee, E.-Y. Park, E.-Y. Park, S. Choi, H. Kim, J. Min, C. Lee, C. Lee, C. Kim, C. Kim, and C. Kim, Biomed. Opt. Express **11**, 752 (2020).
[15]W. Zhang, I. Oraiqat, H. Lei, P. L. Carson, I. EI Naqa, and X. Wang, BME Front. **2020**, 9853609.
[16]M. Xu and L. V. Wang, Phys. Rev. E **71**, 016706 (2005).
[17]X. L. Dean-Ben, A. Buehler, V. Ntziachristos, and D. Razansky, IEEE Trans. Med. Imaging **31**, 1922 (2012).
[18]P. K. Pandey, S. Wang, H. O. Aggrawal, K. Bjegovic, S. Boucher, and L. Xiang, IEEE Trans. Ultrason., Ferroelectr., Freq. Control (published online, 2021).
[19]X. Ma, C. Peng, J. Yuan, Q. Cheng, G. Xu, X. Wang, and P. L. Carson, IEEE Trans. Med. Imaging **39**, 1812 (2020).
[20]J. Jang, J. Kim, H. J. Lee, and J. H. Chang, Sensors **21**, 1217 (2021).
[21]C. Yang, X. Jian, X. Zhu, J. Lv, Y. Jiao, Z. Han, A. Stylogiannis, V. Ntziachristos, G. Sergiadis, and Y. Cui, Sensors **20**, 766 (2020).